2014 IEEE International Conference on Robotics & Automation (ICRA)
Hong Kong Convention and Exhibition Center
May 31 - June 7, 2014. Hong Kong, China

Pouch Motors: Printable/Inflatable Soft Actuators for Robotics

Ryuma Niiyama[1], Daniela Rus[2], and Sangbae Kim[1]

Abstract— **We propose a new family of fluidic soft actuators called Pouch Motors. The pouch motors are developed to create printable actuators for enhancing mass-fabrication of robots from sheet materials using easily accessible tools. The pouch motor consists of one or more gas-tight bladders (called pouches) fabricated by heat bonding. We developed two types of actuators from inflatable pouches: the linear pouch motor and the rotational pouch motor. Our theoretical analysis predicts the static force-length and moment-angle relationships of these actuators under pressure control. We compare the theoretical bounds with actual results achieved using several fabricated devices. We developed a fabrication process of pouch motors using a heat stamping technique that allows mass-manufacturing. We also demonstrate three robot bodies with embedded pouch motors: a parallel gripper, a robotic arm with antagonistic actuation, and legged walking robot with a self-contained miniature pneumatic system.**

I. Introduction

A grand challenge for robotics is reducing the time from a concept to a fabricated robot. Since a functional robot system includes the body structure, actuators, sensors and electric circuits, we wish to develop processes that automate the fabrication of all of these components. The wide availability of 3D printing has fueled a large body of research on automating the fabrication of the mechanical structure of the robot. Layered manufacturing processes such as shape deposition manufacturing (SDM) is one approach to embedding sensors and actuators into 3D structures [1]. Folding and self-folding are another approach to constructing 3D structures from 2D processes–e.g. printing [2][3][4]. Other important aspects of manufacturing automation include computer-aided design and computer-generated design [5]. All these prior processes include manual steps to incorporate the actuators in the body of the robot.

The fabrication of the standard actuators used in robotics (e.g. electric motors, pneumatic/hydraulic cylinders) requires relatively complex machining and manual assembling steps. The fluidic cylinders have a simple structure compared to electric motors. However, the cylinder-piston mechanism inherently requires multiple parts and manual assembling steps. We need modifications to both the fabrication and the structure of actuators in order to automate their fabrication and integration with the mechanical structure of a robot.

The family of pneumatic artificial muscle (PAM) actuators [6] is a promising approach to printable actuators because of simplicity. The McKibben type PAM is the most widely used PAM actuator. It consists of an elastic tube, a braided sleeve, and end fittings. After the invention of the McKibben muscle, researchers have improved the actuator by replacing the tube and sleeve with a single-piece tube with embedded fibers [8][7]. Although the fiber-reinforced tube contributes to the durability and simplification of the assembling process, the manufacturing of the tube still requires delicate manual work using a 3D jig or a mandrel.

In the MEMS field, fluidic actuators have been developed using various fabrication techniques such as micromachining, etching, and lithography [9]. Specifically, a membrane actuator called micro balloon actuator is a widely applied actuator for micro-robotics applications [10][11]. Because of its fabrication method and materials, the output force/moment are neither scalable nor usable by robots beyond the millimeter scale. Moreover, in the micro balloon actuator, the considerable elastic deformation of the micro balloon makes theoretical analysis difficult [12].

In this paper we build on this prior work and demonstrate the automated design and fabrication of pouch motor actuators. We also show that these actuators can be seamlessly integrated with the layered fabrication process of printable robots. We derived theoretical models for the linear mode and the rotational mode of the pouch motor. Using these actuators, we constructed three different robots: a gripper, a robotic arm, and a legged walker. In each case, the fabrication of the robot can be automated and the embedded pouch motor delivers the required function.

II. Pouch Motors

A. Overview

The pouch motors are designed to enhance mass-fabrication of robots from sheet materials using accessible tools. Fig.1 shows the manufacturing process of the robot that includes the pouch motors. Users can employ 2D based printing process by cutting and bonding to materialize the design data of the target system. The actuators are simply layered with the structure. The support structure shown here is made by origami folding, but the structure can be fabricated by other techniques such as machining or 3D printing.

Bonding method for making pouches from sheet materials is an essential part of the fabrication. The bonding methods that we examined are heat bonding, glue, and adhesive tape. We chose the heat bonding with mechanical pressure because it is a rapid and durable bonding method.

B. Function of the Actuators

Pouch motors utilize the mechanical work of the deformation of the inflatable pouches. Changes in length and

[1]Department of Mechanical Engineering, Massachusetts Institute of Technology, 77 Massachusetts Avenue, Cambridge MA, USA.
[2]MIT CSAIL, Massachusetts Institute of Technology, 32 Vassar Street, Cambridge MA, USA.

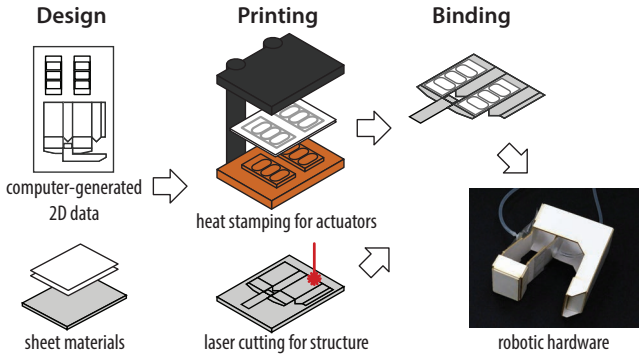

Fig. 1. Overview of the manufacturing process of the robotic system with pouch motors.

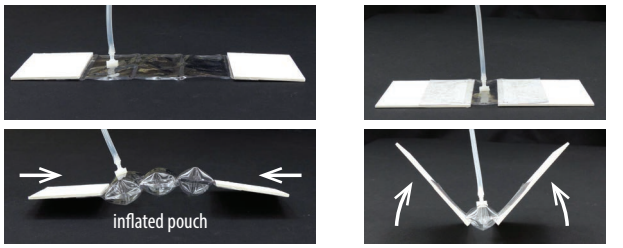

Fig. 2. Prototypes of the linear pouch motor and rotational pouch motor.

curvature are used for linear pouch motor and rotational pouch motor respectively (Fig.2). To extract the mechanical work, at least two fittings are attached on the edges of the pouches

III. Theoretical Model of the Actuators

A. Pouch Model

We developed a mathematical model of the pouch motor Fig.3. The initial state of the pouch with no pressure is a flat square, and the geometry of the pouch under a positive pressure is an airfoil shape with cylindrical surfaces on the top and the bottom of the pouch. As the volume of air inside of the pouch increases, the radius of curvature of the cylindrical surfaces decreases and L decreases. We assume that the membrane of the pouch has zero bending stiffness and is non-extensible. That means there is no elastic energy stored in the membrane. We also assume that the width of the pouch remains constant as it is inflated.

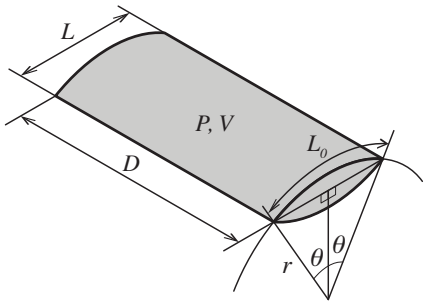

Fig. 3. Model of the pouch.

We can create two types of joint actuation using the pouch: linear mode and rotational mode (Fig.4). The law of conservation of energy and the principle of virtual work are used for the static analysis of two types of pouch motors.

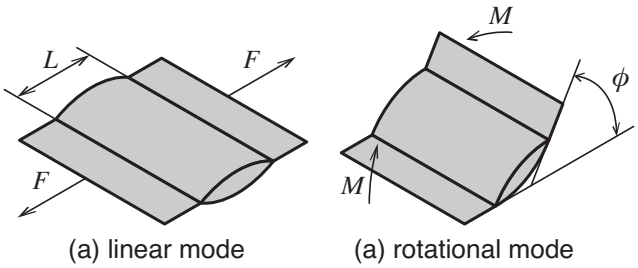

Fig. 4. Model of the pouch in linear mode (a), and rotational mode (b).

The equilibrium between output work dW_{out} and input work dW_{in} corresponding to the virtual displacement is described as the following.

$$dW_{out} = dW_{in} \tag{1}$$

Pressured membranes try to maximize the cross sectional area of the pouch. Assuming the surfaces of the pouch are cylindrical, we obtain equations eq.(2), eq.(3), and eq.(4)

$$L_0 = 2r\theta \tag{2}$$

$$r\sin\theta = \frac{L}{2} \tag{3}$$

$$A = 2r^2\theta - Lr\cos\theta \tag{4}$$

where L_0 is an initial length when the pouch is flat, r is a radius of the curve of the membrane, θ is the central angle of the circular segment, L is a length of the chord or the length of the pouch, and A is the cross sectional area of the pouch.

From eq.(2) and eq.(3), by eliminating the radius r, we obtain the length of the pouch, that is

$$L(\theta) = L_0\frac{\sin\theta}{\theta} \tag{5}$$

The volume of the pouch V can be derived as

$$V(\theta) = AD = \frac{L_0^2 D}{2}\left(\frac{\theta - \cos\theta\sin\theta}{\theta^2}\right) \tag{6}$$

where D is a width of the pouch. We have obtained both the length and the volume of the pouch as a function of the parameter θ, and L_0 and D are constant.

B. Linear Pouch Motor

The work of fluid in the pouch is transformed into tension force F in the case of linear pouch motor. The energy conservation eq.(1) corresponding to a virtual translation dL becomes

$$-FdL = PdV \tag{7}$$

where F is the tension force, P is an inner pressure of the pouch, dL and dV are small displacements in length and volume correspondingly.

We finally obtain the following result.

$$F(\theta) = -P\frac{dV}{dL} = -P\frac{\frac{dV}{d\theta}}{\frac{dL}{d\theta}} = L_0 DP\frac{cos\theta}{\theta} \tag{8}$$

Introduce a quantity L_e as the ratio of total deformation to the initial length.

$$L_e = \frac{L_0 - L}{L_0} = 1 - \frac{sin\theta}{\theta} \tag{9}$$

When $\theta \to 0$, eq.(8) says $F \to \infty$. In reality, the material of the actuator can stretch or yield by the tension force. Therefore, define corrected L_e as

$$L'_e(\theta) = L_e\left(1 + \frac{d\pi}{\pi - 2}\right) - d \tag{10}$$

$$d = C_e P \tag{11}$$

where d is a correction term, and C_e is a coefficient to determine a strain that is in proportion to the pressure. L_e and L'_e cross at the point of $F(\pi/2) = 0$, $L_e(\pi/2) = L'_e(\pi/2) = \frac{\pi-2}{\pi}$. The theoretical maximum contraction ratio of the linear pouch motor is $\frac{\pi-2}{\pi} \approx 0.363$. The maximum force output is observed when $L = L_0$, $L'_e = 0$.

C. Rotational Pouch Motor

The work of fluid in the pouch is transformed into moment (torque) M in the case of a rotational pouch motor. The energy conservation eq.(1) corresponding to a virtual rotation $d\phi$ becomes

$$Md\phi = PdV \tag{12}$$

The output angle ϕ is a function of θ, that is

$$\phi(\theta) = 2\theta \tag{13}$$

We obtain the following result.

$$M(\theta) = P\frac{dV}{d\phi} = P\frac{\frac{dV}{d\theta}}{\frac{d\phi}{d\theta}} = L_0^2 DP\frac{\cos\theta(\sin\theta - \theta\cos\theta)}{2\theta^3} \tag{14}$$

The theoretical maximum range of motion of the rotational pouch motor is π rad (180°). The maximum moment is observed when $\phi = 0$.

IV. Experiments

A. Experimental Setup

We use two types of instruments to measure the static properties of the actuator (Fig.5). The instrument consists of a frame, a force sensor, a potentiometer, and a pressure control system. Testing samples of the actuators are made from PVC sheet with thickness of 4mil (0.102mm). The pouches are manually fabricated by using a line heat sealer.

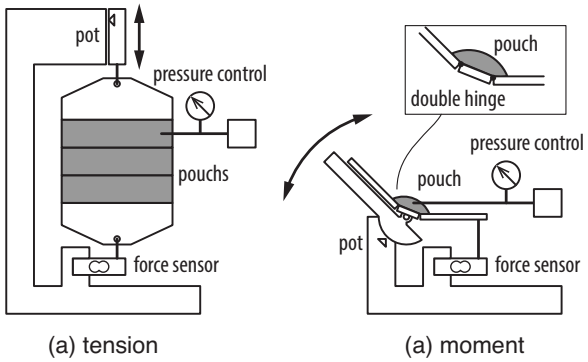

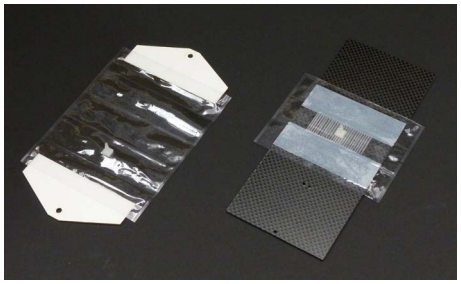

Fig. 5. The experimental setup for tension and moment measurements (top). A linear actuator and a rotational actuator used in the experiments (bottom).

B. Properties of the Linear Actuators

We tested an actuator with three series pouches. The each pouch has the effective width $D = 0.85$ m, the initial length $L_0 = 0.025$ m, and the initial strain $C_e = 5.0 \times 10^{-6}$ Pa^{-1}. The measurement of the tension force is a quasi-static process, which starts shortening from $L = L_0$ and returns to the initial length. The inner pressure of the pouch is sustained constant by feedback control during the experiments.

The comparison between the theoretical and measured force-length properties is shown in Fig.6. The theoretical curves are the parametric plot of the equations eq.(8) and eq.(11) for $0 < \theta \leq \pi/2$. Force F is a monotonically decreasing function of the length L in any pressure and is slightly concave up. The measured data has similar trend with the model. The measured maximum contraction ratio of the linear actuator is about 30% of the initial length in 20 kPa. This value is comparable to McKibben artificial muscle.

We also examined the hysteresis of the linear actuator in continuous five trials (Fig.7). The output forces in the shortening process are always lower than return curves.

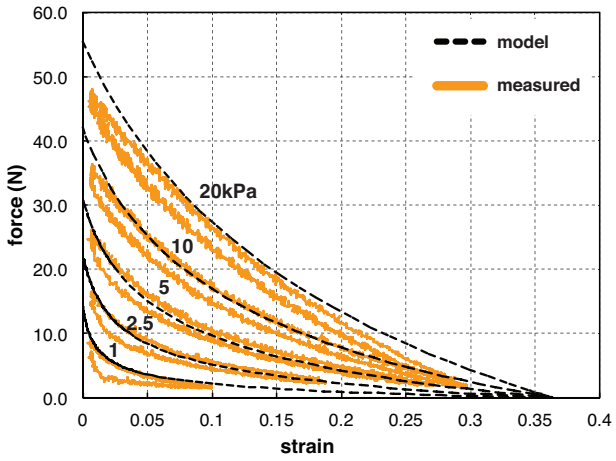

Fig. 6. The force-length relationship of the linear pouch motor at various pressures. Solid lines show measured data and dotted lines show the corresponding theoretical curves. X-axis shows the ratio of the total deformation to the initial length L_0.

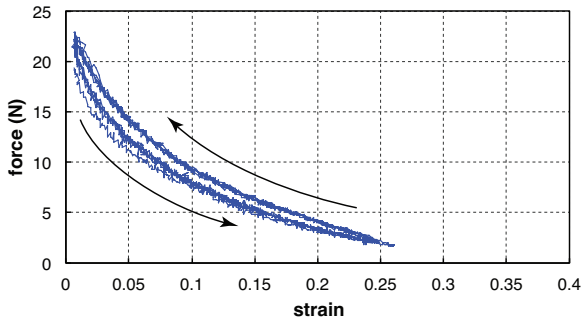

Fig. 7. The hysteresis of the linear pouch motor in five cycles, 5kPa.

C. Properties of the Rotational Actuators

We use a single pouch that has the same parameters used in the experiments of the linear pouch motor. The measurement of the moment is a quasi-static process that starts bending from $\phi = 0$ until $F = 0$ then return to the initial angle. Although, we assume that the pouch always keeps circular shapes in the theoretical model, for practical use, rigid parts attached on the both edges of the pouch can distort the shape of the pouch. In this experiment, we employed a rigid double hinge mechanism to support the actuator (top right of the Fig.5).

The comparison between theoretical and measured moment-angle properties is shown in Fig.8. The theoretical curves are the parametric plot of the equations eq.(14) and eq.(13) for $0 < \theta \leq \pi/2$. Fig.8 also shows a theoretical curves of a single hinge model. The moment M is a monotonically decreasing function of the angle ϕ in any pressure.

D. Fabrication with printing block

We tested heat bonding method that has advantages in strength, sealing performance, and the potential of automation (Fig.9). In the experiments, we used a hot plate to control the temperature of the printing block. The process

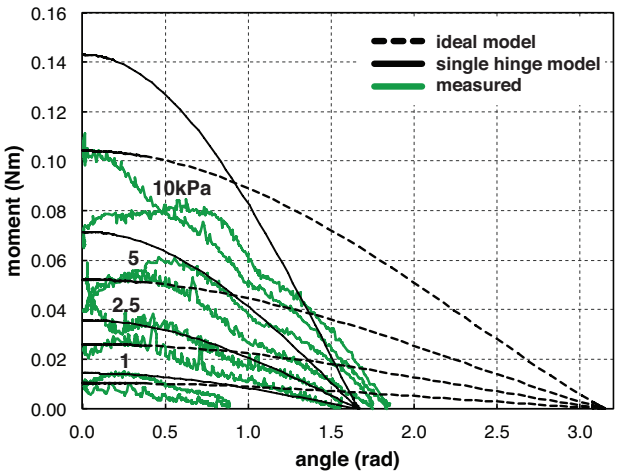

Fig. 8. The moment-angle properties of the rotational pouch motor at various pressures. Green lines show measured data and black lines show the theoretical curves.

of the fabrication is similar to the printing press. A platen covered with a high-temperature silicone rubber press the sheet material to a hot printing block. We used a high-temperature PTFE-coated fabric to prevent plastic sheets from sticking to the printing block.

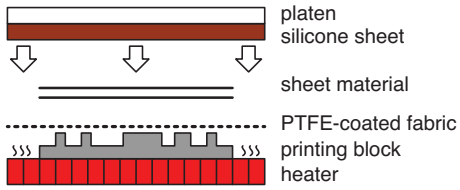

Fig. 9. The printing method with heat bonding.

Fig.10 shows printed pouches with primitive shapes by using proposed heat bonding method. These primitive stamp rings are made from extruded aluminum pipes. We also create a positive printing block by using CNC milling machine from the 2D pattern data (Fig.11). Those printing technique enables the instant mass fabrication of the multiple pouch motors on the sheet materials.

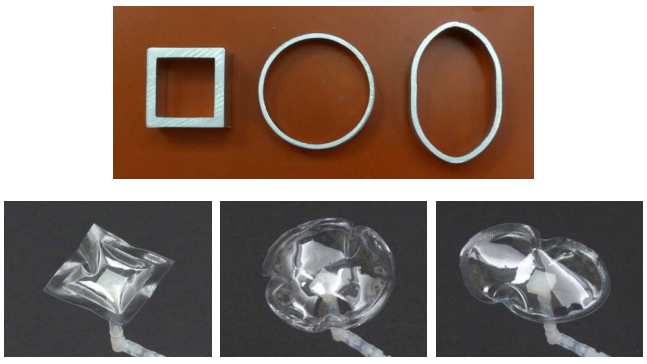

Fig. 10. Aluminum stamp blocks: square, circle, and oval (top). Inflated pouches obtained from the printing process (bottom).

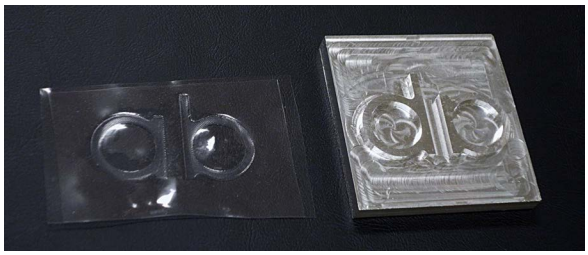

Fig. 11. The CNC milled aluminum printing block and a sample of stamped pouches on the plastic sheet.

V. Applications

A. Gripper

We use pouch motors for driving gripper fingers for manipulating objects. Not only the actuators but the structure of the gripper is also developed from 2D-based fabrication techniques (Fig.12). Two rotational pouch motors are layered on the structure made from paper board. The pouch motors drive the base joints of the parallel mechanism to open/close the jaw (Fig.13).

The weight of the gripper is about 26 g. Maximum gripping force of the prototyping gripper measured by a spring scale is about 2.8 N. The increase of the angle of a joint by inflation leads the decrease of the gripping force. Using the theoretical model introduced in this paper, we can customize the design based on the torque availability and the allowable rang of motion.

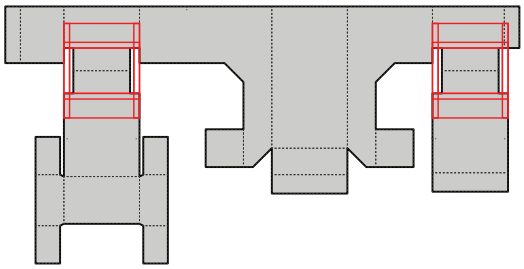

Fig. 12. The unfolded 2D-layer of the gripper. The red squares show the position of the layered rotational pouch motors.

Fig. 13. A gripper prototype driven by two rotational actuator modules.

B. Robot arm

The single joint robot arm is fabricated as an example of the application of the linear pouch motors. Both the base structure and the actuators are manufactured by layered process (Fig.14). The actuator can only generate contraction forces like biological muscles. We use two linear actuators for bidirectional actuation of the joint.

Fig.15 shows swing motion of the arm. Since the actuator is light-weight, has no friction elements, and driven by low-viscosity fluid (air), the actuator is potentially suitable for the rapid motion. Moreover, because the linear actuators can provide sufficient force without transmission, it can be used as direct drive system that can provide back-drivability.

The linear actuator also has non-linear force-length properties. Therefore, by using antagonistic actuation of the joint, we can independently control the stiffness/compliance of the joint as well as angle (Fig.16).

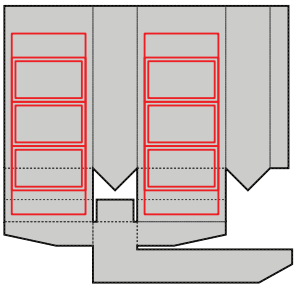

Fig. 14. The unfolded 2D-layer of the robotic arm. Red squares show the position of linear pouch motors.

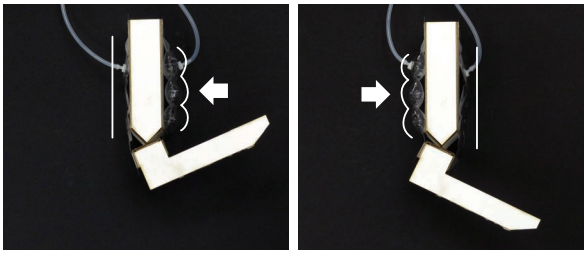

Fig. 15. The swing motion of the robot arm.

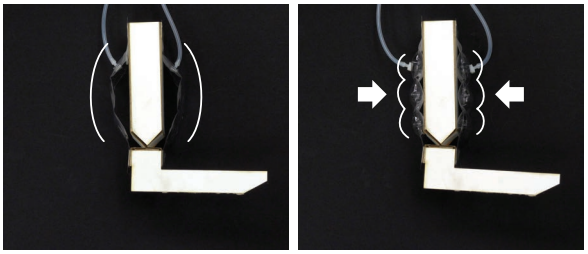

Fig. 16. The stiffness control of the joint of the arm. The free state with zero pressure (left) and the stiff state with pressured pouch motors (right).

C. Legged Robot

Third example is a quadruped robot. The robot has a height of 70mm, and a length of 125mm. The propelling mechanism of the robot is an angled hinge joint on the trunk (Fig.17). The feet are fixed on the body and the angled trunk joint generates twisting motion to lift and swing the feet. Actuators are attached antagonistically on the both side of the hinge

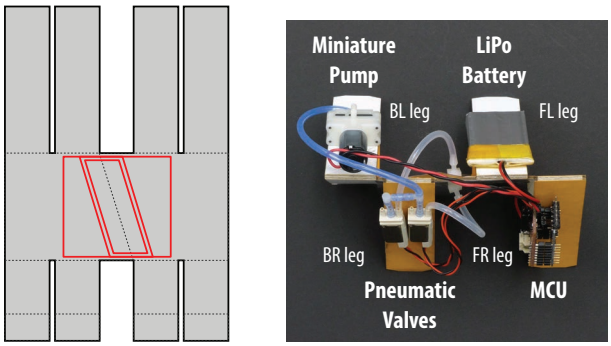

Fig. 17. The unfolded 2D-layer of the legged robot (left). Red squares show the position of the rotational pouch motors. Top view of the robot (right) shows the stand alone miniature pneumatic system.

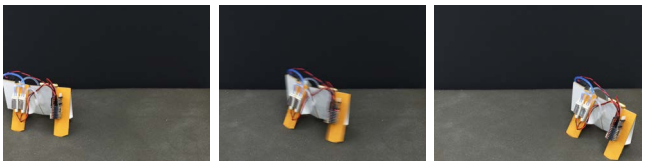

Fig. 18. Walking of the legged robot using the pouch motors (from left to right). Two pouch motors twist the trunk for propelling the robot.

joint. Walking motion on polyurethane foam floor is shown in Fig.18. The walking speed is about 0.45m/min.

In the experiment, a switching sequence of supply phase and exhaust phase is used as the motor command. Fig.19 shows the sequence and measured inner pressure of the pouch motor on right side. The pressure data has a two-peak profile per step. The first peak shows rapid pressure increase because the volume of the pouch is small under low angle. The second peak shows that the inflation of the pouch reaches the limitation.

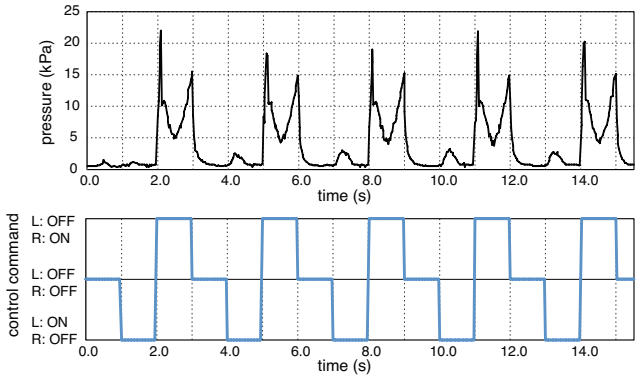

Fig. 19. The command sequence and the pressure profile of the pouch motor on right side.

The movements of pneumatically-driven robots are usually limited by stationary air compressor placed outside the robot. We develop a self-contained pneumatic control system includes a miniature pump, valves, a micro controller, and a battery pack (Fig.17).

VI. Conclusion

We introduce a new printable soft actuator. Unlike other actuators that are assembled separately, this pouch motors can be integrated with other structural components of printable robot via layered manufacturing process. We provide first comprehensive studies of the actuators: function, theoretical analysis, fabrication method, and application examples. The fabrication method introduced here is suitable for making complicated shapes of pouches from computer-aided design. With further development, this technique will enable mass production of smart printable robots that contain structure, sensors, electronics and actuators.

References

[1] S. A. Bailey, J. G. Cham, M. R. Cutkosky, and R. J. Full, "Biomimetic Robotic Mechanisms via Shape Deposition Manufacturing", Design, pp. 321–327, 1999.

[2] A. M. Hoover and R. S. Fearing, Fast scale prototyping for folded millirobots, vol. 5, no. April 2005. Ieee, 2008, pp. 886–892.

[3] E. Hawkes, B. An, N. M. Benbernou, H. Tanaka, S. Kim, E. D. Demaine, D. Rus, and R. J. Wood, "Programmable matter by folding", Proceedings of the National Academy of Sciences of the United States of America, vol. 107, no. 28, pp. 12441–12445, 2010.

[4] C. D. Onal, R. J. Wood, and D. Rus, Towards printable robotics: Origami-inspired planar fabrication of three-dimensional mechanisms. IEEE, 2011, pp. 4608–4613.

[5] H. Lipson and J. B. Pollack, "Automatic design and manufacture of robotic lifeforms", Nature, vol. 406, no. 6799, pp. 974–978, 2000.

[6] F. Daerden and D. Lefeber, "Pneumatic Artificial Muscles : actuators for robotics and automation", European Journal of Mechanical and Environmental Engineering, vol. 47, no. 1, pp. 11–21, 2002.

[7] F. Daerden and D. Lefeber, "The concept and design of pleated pneumatic artificial muscles", Most, vol. 2, no. 3, pp. 41–50, 1999.

[8] D. Bergemann, B. Lorenz, A. Thallemer, "Actuating Means", U.S. Patent 6 349 746 B1, Feb. 26, 2002.

[9] M. De Volder and D. Reynaerts, "Pneumatic and hydraulic microactuators: a review", Journal of Micromechanics and Microengineering, vol. 20, no. 4, p.043001, 2010.

[10] F. Kawai, P. Cusin, and S. Konishi, Thin flexible end-effector using pneumatic balloon actuator, vol. 89. 2000, pp. 28–35.

[11] Y. Lu and C.-J. K. C.-J. Kim, Micro-finger articulation by pneumatic parylene balloons, vol. 1. Ieee, 2003, pp. 276–279.

[12] B. Gorissen, M. De Volder, A. De Greef, and D. Reynaerts, "Theoretical and experimental analysis of pneumatic balloon microactuators", Sensors and Actuators A: Physical, vol. 168, no. 1, pp. 58–65, 2011.